Simulation of the vibrations produced by extended bearing faults in gearboxes

N. Sawalhi and R.B. Randall

School of Mechanical and Manufacturing Engineering, The University of New South Wales, Sydney 2052, Australia

ABSTRACT

Dynamic simulations of gears and rolling element bearings have previously been made separately, but cases have been experienced in practice where bearing faults show up only because they modulate the gearmesh signal in a way that is different from the effects of gear faults. A combined gear/bearing model has been made to obtain a better understanding of the interaction of the two components. Results have previously been published for simulated local faults in the bearings. The simulation model has now been modified to model extended faults of the type that do not necessarily produce high frequency impact responses, but do modulate the gearmesh signals. This simulation model will be useful to test new diagnostic algorithms, as well as prognostic algorithms by varying the size of the simulated faults. A third application is to use the simulated signals to train neural networks to recognize the various faults without having to experience large numbers of failures. The paper compares simulated and actual signals (localized and extended inner race faults) from a gear/bearing test rig, and in particular demonstrates that they react similarly to existing diagnostic techniques.

INTRODUCTION

Gears and bearings are kinetically coupled components, which interact with each other as the meshing forces of the gears are supported by the bearings.

In the simplest cases (localized bearing faults), this interaction is additive, and the separation of the two signals (bearing signal and the gear signal) can be achieved by using synchronous averaging, Self-Adaptive Noise Cancellation (Ho, 1999) or Discrete Random Separation (DRS) (Antoni and Randall, 2004). The basis of separating the two signals is that the gear signal is periodic while the bearing signal contains some randomness due to the slippage of the rolling elements as a result of load angle variation. Moreover, due to the additive nature of the interaction, bearing signals prevail over certain frequency ranges and can be detected using envelope analysis (High Frequency Resonance technique) (McFadden and Smith, 1984 A), which has recently been automated using spectral kurtosis (Antoni and Randall, 2006, Sawalhi and Randall, 2005). Experiments and simulation on the University of New South Wales (UNSW) test rig have clearly supported this point (Ho, 1999, Antoni and Randall, 2002, Sawalhi et al. 2006 A, B).

Different cases have been encountered where localized faults extend beyond the spacing between two rolling elements and are smoothened by the successive passing of the rolling elements, so that no impulses are generated (Antoni and Randall, 2002). The interaction between the gear signal and the bearing signals in such cases is no longer additive, but is largely multiplicative, meaning that the separation may no longer be straightforward as in the case of localized faults. In such cases, the bearing fault manifests itself by modulating discrete frequencies, such as gearmesh–related frequencies (Antoni and Randall, 2002). Different examples of actual and analytically simulated signals from gearboxes were presented by Antoni and Randall (2002). The illustrated examples showed the differences in the case of localized and distributed faults, and proposed a way of distinguishing between the two using cyclostationarity.

This paper presents a combined dynamic model for gears and bearings, in which an extended fault in the rolling element bearing can be studied in the presence of gear interaction. The new simulation model is in fact an update of an earlier presented model (Sawalhi et al. 2006 A) intended to study the interaction in the presence of localized faults (inner and outer race). Fault simulation can be very valuable in machine diagnostics and prognostics in order to produce signals with well-defined characteristics rather than waiting until such signals arise randomly. For example, such signals could be used to train neural networks to perform diagnostics and prognostics of developing faults in machines. These usually require so much data to train them that it would not be economical to actually experience the number of faults of each type required to accomplish the training.

The current paper illustrates how the rough surface topography of an extended fault can be generated and incorporated in the bearing function, reviews the combined bearing/gear model and discusses the nature of the bearing signals from the perspective of cyclostationarity. The simulated signals for an extended inner race fault, a localized inner race fault and a good bearing (all with added pink noise) are analysed using the procedure (spectral correlation) proposed in Antoni and Randall (2002).

Analytical Models of Localized Faults in Rolling Element Bearings

Rolling element bearings exist in a broad range of applications across almost all industries. Through their life, they support the rotating parts, and interact closely with them. This close interaction, along with the background noise, acts in most cases as a mask to the vibration signature, and thus complicates their health monitoring.

One important characteristic of the vibration generated by the failure in the rolling element bearings in the early stages (local surface damage) is that it is impulsive. Impulses are created when a defect (local spall) on a rolling surface impacts with another surface.

A traditional way of modelling localized bearing faults is as a sequence of high frequency bursts, which represent the impulse response of the signal transmission path, repeated at a rate given by the fault interacting with the rolling elements, whether it is on the inner race, outer race or rolling elements (McFadden and Smith, 1984 B). The rolling element and inner race faults experience a variation of the load while passing through the load zone. This has the effect of modulating the impulse train by either the cage speed (rolling element fault) or the shaft speed (inner race fault) (McFadden and Smith, 1984).

This model was realistically updated by Ho and Randall (2000), by varying the spacing between the bursts randomly by a small percentage, which happens in practice as a result of fluctuations in the load angle, and the tolerances of the cage. The importance of this is shown in figure 1, which shows the effect of introducing a small random fluctuation (0.75 %) using simulated signals (outer race). Note how the direct spectrum of the original signal (in terms of acceleration) contains almost no information at the low frequencies about the pulse spacing. In the vicinity of the resonance, this information can be extracted when no random fluctuations exist, but is impossible with a small amount of random fluctuation, as the harmonics smear into one other. Figure 1 also shows the advantage of envelope analysis in revealing the average pulse frequency, even with some fluctuations.

Another way of looking at the signals from localized faults is through cyclostationarity (a cyclostationary process is a random process with a periodic autocorrelation function (Gardner, 1986)). Bearing signals with local faults are described as being approximately cyclostationary (pseudo-cyclostationary) due to the fact that they don't have a defined mean period, and consequently their autocorrelation function is not truly periodic, because of the nonstationarity in the inter-arrival times of the successive impacts (as a result of the slippage) (Antoni and Randall, 2002). This has the effect of smearing the higher harmonics as previously explained in connection with figure 1.

Although the above models shed light on the nature of the vibration signal from a faulty bearing, they do not include the physical properties of the system (stiffness, damping, dimensions of the rolling bearings, etc…) and cannot then be incorporated dynamically in a given system.

Dynamic Simulation of Rolling element bearings

To address the issue of modelling rolling element bearings in a dynamic manner, Fukata et.al (1985) introduced a two degree-of-freedom (2 DOF) system, which provides the load-deflection relationships, while ignoring the mass and the inertia of the rolling elements. Contact forces (based upon a Hertzian contact relationship (Harris, 1966)) are summed over each of the rolling elements to give the overall forces on the shaft. The stiffness of the bearing model (Figure 2) is both non-linear and time varying, but can still be incorporated into dynamic models.

Building on Fukata's model, Feng et.al (2002) presented a bearing–pedestal model (4 DOF model), which took into consideration the slippage of the rolling elements and the possibility of a localized fault on either the inner or outer races.

The model is based on calculating the deflection δ_j at each rolling element j (total number of elements (n_b)).

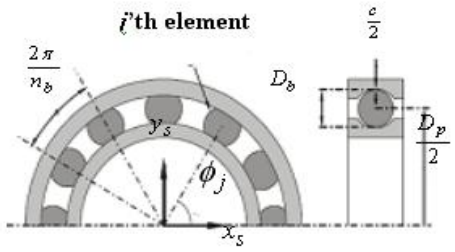

Figure 2 Rolling Element Bearing Two degree of freedom model (Liew et.al, 2002)

The deflection, which is defined in equation (1), takes into consideration the loading status of the rolling elements (represented by the contact switch γ), and the location of the rolling element with respect to the fault region (fault depth defined using a step function C_d and a fault switch β, which is activated for the elements in the spall region). More over, the clearance (c), and any unbalance can be represented in the net force.

$$\delta_j = (x_s - x_p)\cos\phi_j + (y_s - y_p)\sin\phi_j - c - \beta_j C_d \quad (1)$$

Where: x_s, y_s: Displacements of the inner race in the horizontal and vertical directions respectively

x_p, y_p: Displacements of the pedestal in the horizontal and vertical directions respectively

ϕ_j: The position of the element j

The ball raceway contact force (f) is calculated using traditional Hertzian theory (non-linear stiffness) (Harris, 1996) from:

$$f = k_b \delta^n \quad (2)$$

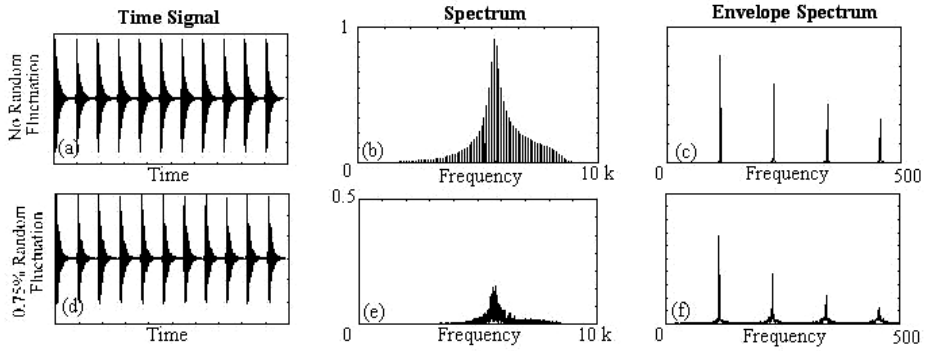

Figure 1 Bearing fault pulses (outer race fault) with and without random fluctuations (Ho and Randall, 2000)

The load deflection factor (k_b) depends on the contact geometry and the elastic constants of the material, and exponent n = 1.5 for ball bearings and 1.1 for roller bearings. Using equation (2) and summing the contact forces in the x and y directions for a ball bearing with (n_b) balls, the total force can be calculated as:

$$f_x = k_b \sum_{j=1}^{n_b} \gamma_j \delta_j^{1.5} \cos\phi_j \quad (3)$$

$$f_y = k_b \sum_{j=1}^{n_b} \gamma_j \delta_j^{1.5} \sin\phi_j \quad (4)$$

The stiffness of the bearing as presented by this model is non-linear, and is time varying in nature as the positions of the rolling elements (function of time) determine the overall contact.

The random fluctuation of the ball positions as a result of the slippage can be either forward or backward of the mean. This was related to the nominal motion of the cage ($\omega_c dt$) and was modelled by introducing random numbers of zero average with evenly distributed fluctuations within $\phi_{jrand} = \pm 1.5\omega_c dt$ (Feng et.al, 2002).

Feng's model was further updated by Sawalhi et.al (2006), by introducing an extra degree of freedom (sprung mass system to excite a typical high frequency resonance of the system) and by changing the way of modelling the spall (the way of defining the variable C_d); so that rollers lose and gain contact gradually. The new five degree-of-freedom model is shown in figure 3. It was implemented in a gear dynamic model using Simulink® as an S-function (special function for Simulink®), which was dynamically updated as the simulation proceeded.

The details of the new model as well as the results for an inner race and outer race faults were presented in Sawalhi et.al (2006) in two conference papers (IFToMM 2006 and COMADEM 2006). The former concentrates on illustrating the models and shows how the impulse itself is formed of two parts (entry and exit to the spall region), while the latter shows how an inner race fault can be separated based on the randomness of pulse spacings as a result of the slippage. Both papers showed how both simulated and actual results have the same behaviour.

Modelling extended faults

A rough surface can be treated as a series of discrete points. The heights of these points are modelled as a random variable. The distribution of the heights gives important information about the surface (a rough surface will have a large standard deviation) (Wu, 2002). A large number of parameters have been proposed for describing the roughness of a surface, however the most common of these, the root mean squared value (rms) roughness (h) is the standard deviation of surface heights (Wu, 2002).

The procedure of generating the rough surface for this model ($C_d(\phi)$) includes three main steps, and can be described as follows: -

1. Gaussian noise is generated using the function *randn* in Matlab® and is scaled to the required surface roughness by multiplying by h (a value ranging from 10 μm to 20 μm is selected).
2. The generated random noise is low pass filtered to fit the rolling element to the path it can practically reach (rolling element touches only at the asperities). The wavelength λ (inverse of the low pass filter frequency) is derived as in equations (5-8) using the terminology explained in figure 4. The low pass filtered signal is shown in figure 5 along with the original signal (Gaussian noise).

At $x = \frac{3\lambda}{4}$ the curvature is the same for both the rolling element (ball) and the surface, which also means that the ball can roll between the two peaks.

The curvature of the ball (k_{ball}) can be estimated using equation (5), while that of the sinusoidal surface (k_{si}) defined in figure 4 at $x = \frac{3\lambda}{4}$ is given in equations (6 and 7)

$$k_{ball} = \frac{2}{D_b} \quad (5)$$

$$k_{si} = \frac{|f''(x)|}{|1 + f'(x)^2|^{3/2}} \quad (6)$$

$$k_{si(x=\frac{3\pi}{4})} = \frac{4a\pi^2}{\lambda^2} \quad (7)$$

The wavelength (λ) for an equal surface curvature can be found by equating equations (6) and (7) as: -

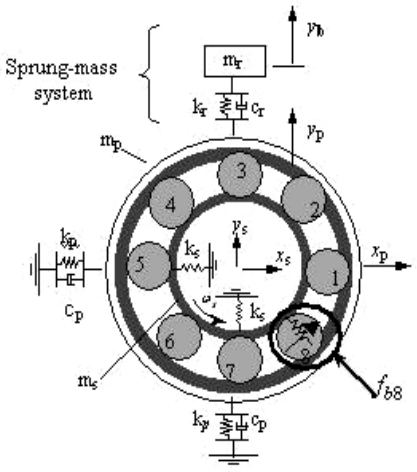

x_s, y_s: Shaft/inner race DOF
x_p, y_p: pedestal/outer race DOF
y_b: Measured vibration response
k_p: pedestal stiffness
k_s: shaft Stiffness
k_r: Stiffness of sprung system
c_p: Damping in pedestal
c_r: Damping in sprung system
m_s: Mass of shaft/inner race
m_p: Mass of pedestal
m_r: Mass of resonance changer
ω_s : Shaft rotational speed
f_{b8}: Ball race way contact force for element 8

Figure 3 Five degree-of-freedom bearing-pedestal model (Sawalhi et.al, 2006 A)

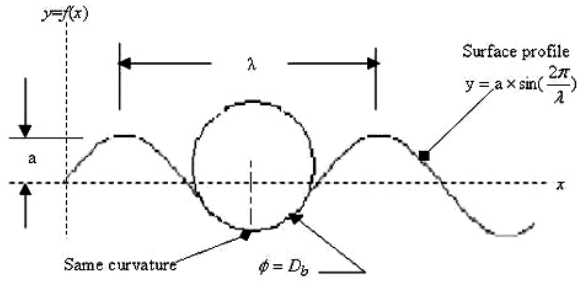

Figure 6 Wavelength derivation

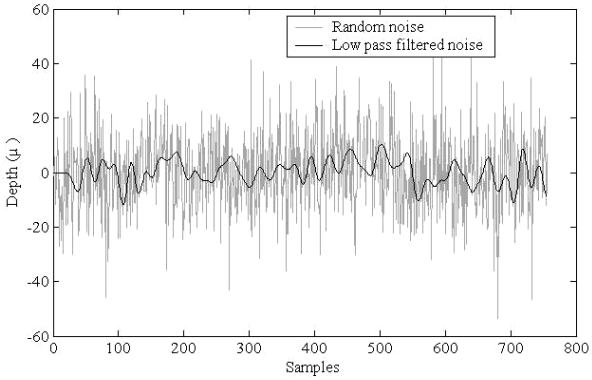

Figure 6 Low pass-filtered signal (dark colour)

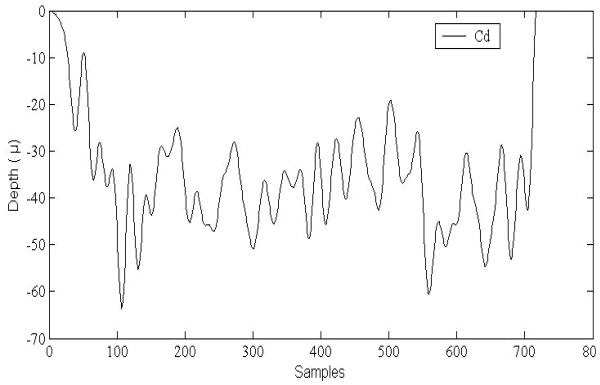

Figure 6 Final rough surface plots

$$\lambda = \pi\sqrt{2aD_b} \tag{8}$$

3. Spalling leaves deep cavities at contact surfaces with a depth of 20 μ m to 100 μ m (Bruce, 2004). In order to represent this topography, the low pass filtered signal generated from the first two steps is superimposed on a bucket shaped surface (depth of 20 μ m to 100 μ m) to give the final topography of the rough surface as shown in figure 6.

Cyclostationary Analysis

When an extended fault exists on the inner race, it periodically enters and exits the load zone, and the resulting signal (non impulsive, with randomly distributed phases) is modulated by the shaft speed. This has been described as a purely cyclostationary process (Antoni and Randall, 2002) as opposed to the pseudo-cyclostationary process associated with the localized faults.

Based on these views of cyclostationarity, an approach based on the properties of cyclostationary processes has been suggested by Antoni and Randall (2002), which showed how to distinguish the modulation associated with a bearing fault from that associated with a gear fault.

The Autocorrelation function of the signal $x(t)$ can be defined as (Gardner, 1991): -

$$R_x(t,\tau) = E[x(t+\tau/2)x^*(t-\tau/2)] \tag{9}$$

Where E [.] is the mathematic expectation operator, τ is the time lag. For stationary signals, there is no variation with the time *t*, and the autocorrelation function can be written as $R_x(\tau)$. For cyclostationary signals, there is a periodic variation with the time *t*, and there is an advantage in performing a two-dimensional Fourier transform of the autocorrelation function with respect to the two time variables (t,τ), to give the so called S*pectral Correlation Function* (SCF) defined by (Antoni and Randall, 2002): -

$$S_{xx}(\alpha,f) = \underset{\substack{t\to\alpha \\ \tau\to f}}{F}\{R_x(t,\tau)\} \tag{10}$$

The SCF is a powerful tool in distinguishing between the different types of signals, viz, stationary, cyclostationary and periodic and as a result identifying the source of fault. The main characteristics given by this process are as follows: -

- Stationary random signals - do not change with time *t*, and then will only have a component at zero cyclic frequency (α = 0), which is the normal power spectrum.
- Periodic signals - these will have discrete components in both frequency directions (α, f), thus being made up of a "bed of nails".
- Cyclostationary signals - these will be continuously distributed in the f direction but discretely distributed in the α direction.

Thus if the SCF is evaluated at a cyclic frequency (α) coinciding with one of the discrete components other than zero, it will not be contaminated with stationary noise, but on the other hand will be continuous for cyclostationary signals and discrete for periodic signals. If discrete frequency components are first removed by DRS, only the cyclostationary components will be left.

The UNSW spur gear test rig

The gearbox test rig (figure 7) under investigation was built by Sweeney (1994) to investigate the effects of gear faults on transmission error. In this test rig, the single stage gearbox (in this case a spur gear set with 1:1 ratio and 32 teeth on each gear) is driven primarily by a 3-phase electric motor, but with circulating power via a hydraulic pump/motor set. The input and output shafts of the gearbox are arranged in parallel and each shaft is supported by two double row ball bearings (Koyo 1205). The flywheels are used to reduce the fluctuations of the input and output shaft speeds. The couplings are flexible in torsion and without stiffness in bending, making them very helpful for attenuation of the shaft torsional and lateral vibration.

The UNSW Dynamic simulation Model

The modelling of the dynamics of the UNSW gear test rig is accomplished by translating the physical components of interest into a schematic presentation as shown within the dotted box in figure 7. These have been selected based on previous recommendations on the importance, relevancy and contribution to the dynamics of the model (Sweeney, 1994, Du, 1997 and Gao, 2000).

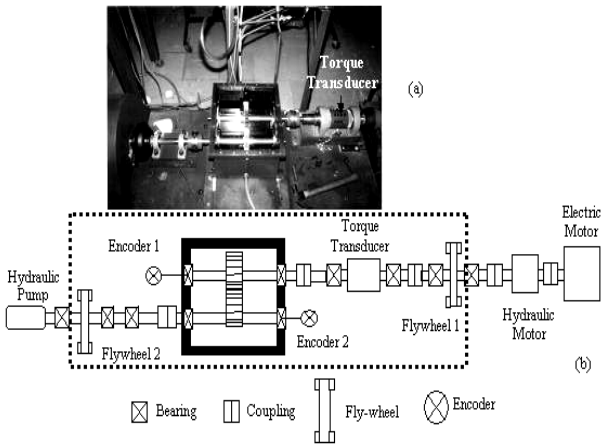

Figure 8 (a) Spur gear test rig (b) schematic diagram of the spur gearbox rig (Sawalhi et.al, 2006 A)

A lumped mass parameter model was then constructed to represent the different parameters of the model (stiffness, damping and masses) in both translational and rotational degrees of freedom. Both the 5-DOF bearing model and the gear model were incorporated in the overall model.

There are 34 DOF in the new model as opposed to the 16 DOF in a previous model (bearing modelled as a single degree of freedom system with constant stiffness)]. This is illustrated in the schematic diagram of figure 8. The extra (18) degrees of freedom are due to the inclusion of the 5 DOF bearing model (figure 3), and to the fact that translational degrees of freedom are now considered both along the line-of-action (LoA) and perpendicular to it.

The main assumptions on which the new model is based are as follows: -

1. Shaft mass and inertia are lumped at the bearings or at the gears.
2. Translational degrees of freedom are considered along the LoA and perpendicular to it, with the LoA aligned vertically.
3. Only two resonances of the gearbox casing are considered.
4. The static transmission error of the gears (geometric and elastic) is included.
5. Friction between the gear teeth is neglected.
6. The gearmesh is assumed free from contact loss.

Matlab® matrix capability, and Simulink® simulation environment were employed to solve the set of the equations of motion using the ordinary differential equation solver (ode45). The bearing model was implemented as an S-function (special function for Simulink®), which was dynamically updated as the simulation proceeded. On the other hand, the load dependent non-linearity of the gearmesh stiffness was implemented as a "look-up table" with cubic spline interpolation (Endo, 2005)

Results and Discussion

Simulated signals for an extended fault (one third of the inner race), a localized fault (slot with a width of 0.8 mm) and a good bearing were obtained from the gear/bearing simulation model. The signals were generated at a sampling rate of 48 kHz and with a Signal to Noise Ratio (SNR) of 12 dB. The shaft speed (Ω) was set to 10 Hz and the rate at which rolling elements pass the fault on the inner race (BPFI) is estimated at 71.2 Hz.

Figure 9 shows one complete revolution (4800 samples) for the two cases of the fault, viz extended on the left and localized on the right. The separation of the raw signal (top row) into a periodic signal (gear related component) – middle row - and a bearing related component - bottom row - was achieved using DRS. In both cases, it is seen that gear signals are well extracted, and the residuals reflect the nature of the embedded faults.

The residual is impulsive for the localized fault (characterized by three impulses, with the maximum being centred in the load zone). For the extended fault it is no longer impulsive, but rather has a randomly distributed phase, since the rolling elements are on different positions on the rough surface every revolution.

Figure 10 explores the cyclostationarity for the residual signals (bottom row of figure 9) by evaluating the spectral correlation function (SCF) as discussed earlier in the section on

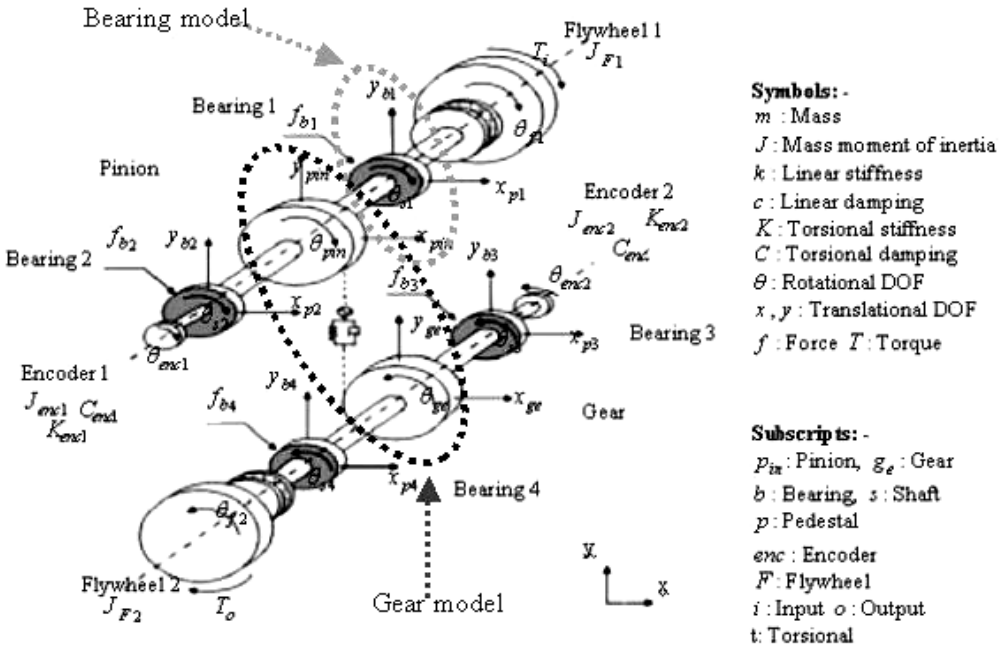

Figure 7 34 DOF dynamic model of the test rig (Vertical direction y aligned with the LoA of the gears) (Sawalhi et.al, 2006 A)

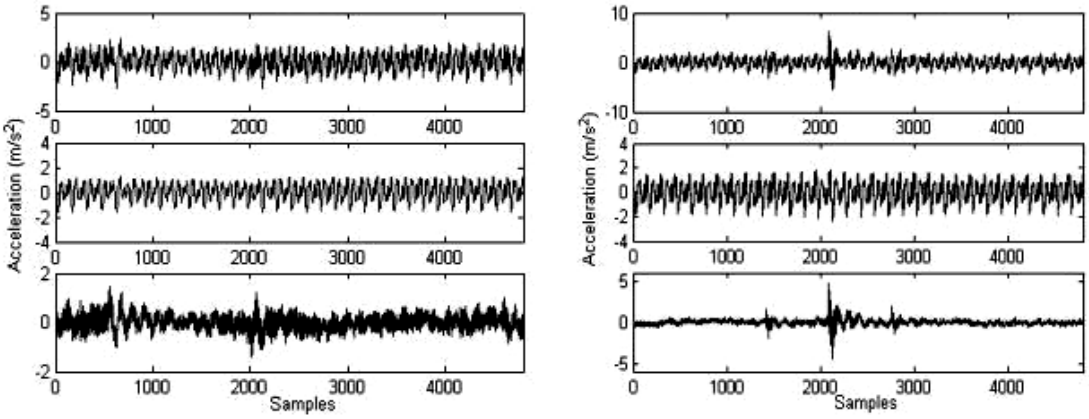

Figure 9 Signal Separation for extended and localized inner race faults. Left: Extended, Right: Localized. Top row: Raw signals, Middle row: Periodic signals (gear), Bottom row: Faulty bearing signals (Residuals).

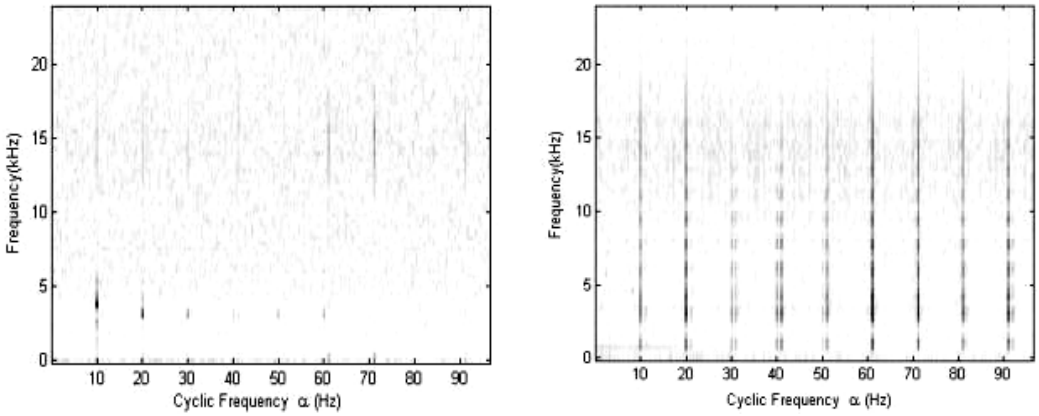

Figure 10 Spectral Correlation Function (SCF). Left: Extended fault. Right: Localized fault.

cyclostationarity. The presentation of the SCF is plotted as an image whose x-axis represents the cyclic frequencies (α) and the y-axis represents the frequency range of the signal. For the extended fault (left side), it is noticed that the SCF is continuous for $\alpha = \Omega$ and has its highest value (darkest part) near 3 kHz. It is also showing at 15 kHz but with smaller values (light colour). It is noticed also that the second and the third harmonics of the shaft speed as well as the BPFI at 71.2 Hz show, but with small values (light colour). On the other side, the localized fault shows high components extending over a wide range of frequency for $\alpha = \Omega$ and its harmonics, as well as α = BPFI and its sidebands.

Figure 10 gives a clear idea about the cyclostationary components in the system, and it has been shown (Randall et.al, 2001) that the integration of the SCF over the whole frequency range (*f*) is equal to the Fourier transform of the mean squared signal (the spectrum of the squared envelope signal). It also serves the purpose of choosing the values of the cyclic frequency (α) to perform the spectral density comparisons. Clearly figure 10 suggests using the shaft speed ($\alpha = \Omega$) for both the localized and extended faults. Such comparisons are shown next in figure 11 for both the raw and residual signals at ($\alpha = 0$) and ($\alpha = \Omega$).

Figure 11.a compares the power spectral density at $\alpha = 0$ (normal power spectral density comparison) for the raw signals, i.e. without removing the periodic part (top row signals of figure (9). There is a significant dB difference for the localized fault case, but not for the extended fault. In both cases the low frequency range (up to 5 kHz), which is dominated by the gear contribution, isn't clearly affected as a result of the fault. No conclusions could be made at this stage, due to the contribution of the noise and the gear signal.

When comparing the power spectral density for the same raw signals but at ($\alpha = \Omega$) as shown in figure 11.b, it is noticed that the dB difference is greatly affected in the high frequency region (away from the gear dominance region). The improvement is due to the fact that no noise effect is present in the signal, as earlier discussed (stationary noise will only show at $\alpha = 0$ but not at any other frequencies). Of importance also to note is the effect in the lower frequency range due to the removal of the noise contribution, which shows how the two main resonances at the lower region show an increase in the dB difference. However, as the gear components aren't removed yet, no conclusion could be drawn to whether this increase of the dB difference is the result of a gear or a bearing fault.

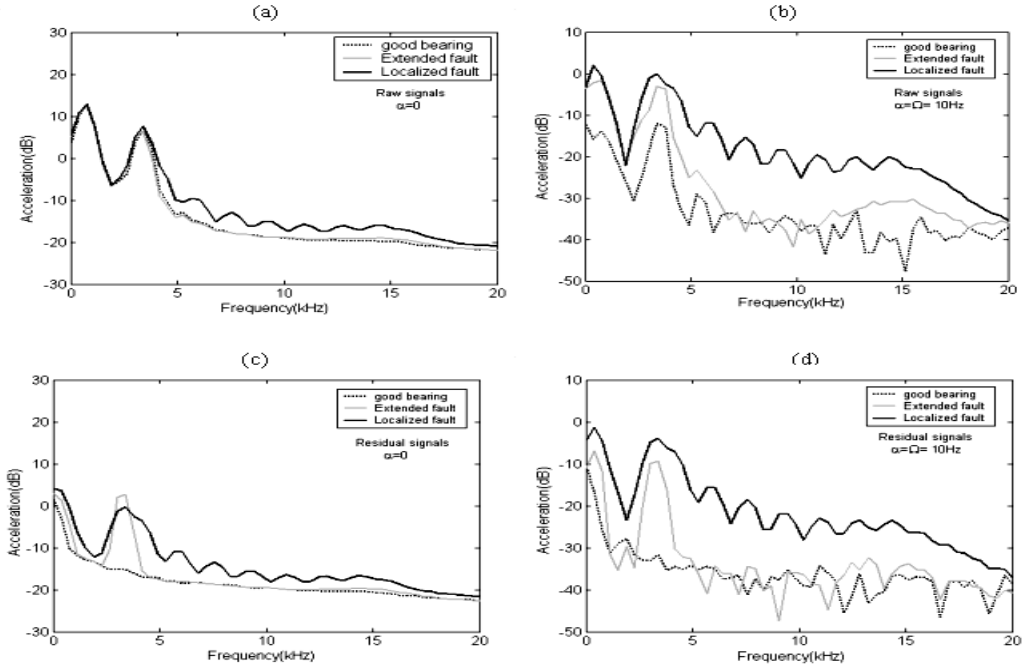

Figure 11 Spectral Correlation at particular values of cyclic frequency α with and without the bearing faults. (a) Raw signals at α = 0. (b) Raw signals at α = Ω (c) Residual signals at α = 0. (d) Residual signals at α = Ω

For the cases of the residual signals (Gear components removed by DRS) at α = 0 and at α = Ω (figures 11.c and 11.d respectively), it is noticed that, by removing the gear contribution, for the both cases of α, there is a great increase in the dB difference, as a result of introducing the faults, but is more noticeable at (α = Ω) due to the absence of the stationary noise. It is clear for this specific case (spectral correlation comparison for the residual signal at α = Ω) that the increase of the dB difference is certainly coming from a bearing fault. Note that for the localized fault, this increase spreads across the whole spectrum (additive interaction), while that for the extended fault mainly affects the resonances in the structure and in particular those in the low frequency range (below 5 kHz), where its effect is due to modulating certain gearmesh frequencies (multiplicative interaction).

Figure 12 compares the spectral correlation at α=0 and α=Ω for actual measured signals from the UNSW test rig. The comparison is made for the residual signals (periodic parts removed using synchronous averaging). The similarities between the simulated (figures 11.c, 11.d.) and measured signals (Figures 12.a, 12.b) are clearly seen for both values of α, however, a few issues need to be addressed due to the assumptions embedded in the simulation model. The first is the high dB difference at α=0 for measured signals compared to simulated ones. This is associated with an increase in the stationary noise level after the introduction of the faults (note that in the simulated signals, the same amount of noise (*additive noise*) was added to all signals, while in measured signals both additive and multiplicative noise are present in the signal). The second is the way the bearing fault manifested itself. This can be seen clearly from figure 12.b, as a multiplicative interaction in the case of the extended fault and an additive interaction in the case of the localized fault. In the simulated signals (figure 11.d), it is noticed that there is a high dB difference in the low frequency region, due to the absence of any source of excitation to the structure in the good bearing case after the removal of the gear components (in the actual measured signals random impacts resulting from the imperfect bearing surfaces excite the resonances of the structure, and can be traced in the residual signals).

The conclusions drawn from the simulated and measured results from the UNSW test rig, and in particular those presented in figures 11.c, 11.d and 12.b agree quite interestingly with actual measurements as shown in figure 13, which presents a case from an actual gearbox of a Sea Hawk Helicopter, where evidence of a distributed bearing inner race fault was reported (Antoni and Randall, 2002). The comparison is

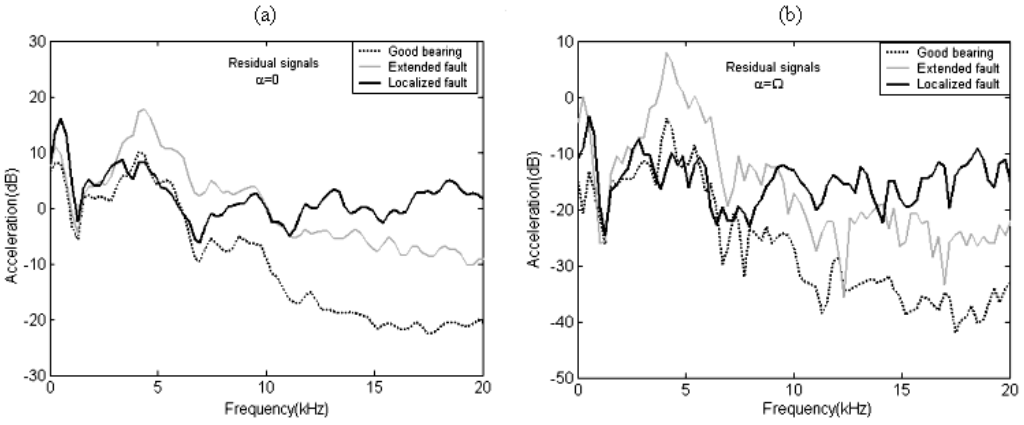

Figure 12 Spectral Correlation at particular values of α with and without the bearing faults for the measured signals. (a) Residual signals at α=0 (b) residual signals at α=Ω

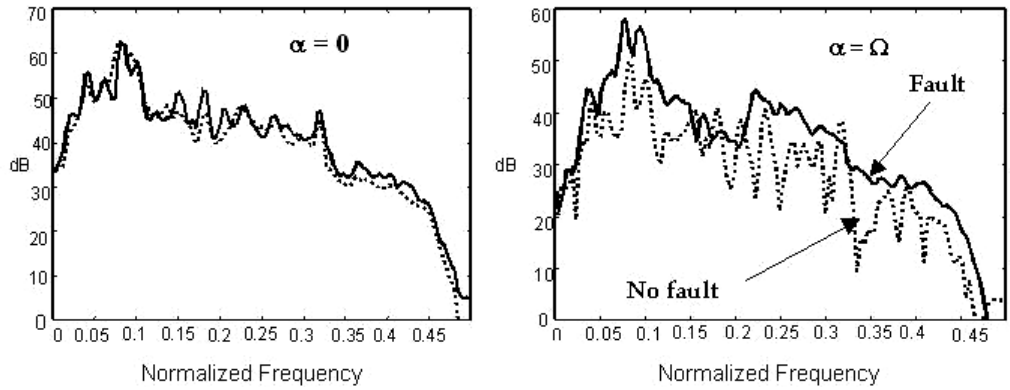

Figure 13 Spectral Correlation at particular values of cyclic frequency α with and without the bearing faults (Actual signals from a gearbox: Antoni and Randall, 2002). Left: α =0. Right: α= Ω

made for the cases of α = 0 (left) and α = Ω (right) for the residual signals. For the former, there is little difference because of the effect of stationary noise, while for the latter, the increase and the smoothing over many frequencies, points clearly to the presence of a cyclostationary component, which most certainly is coming from a bearing fault (as gear components were removed, and there is no masking noise).

Conclusion

This paper presents the results of simulating an extended inner race fault in one of the rolling element bearings in a single stage gearbox. The simulated results of the dynamic gear/bearing model were compared with a simulated localized inner race fault, and were both subjected to the same diagnostic techniques (namely DRS and SCF). The obtained results agrees quite well with results obtained from actual measurements, and show how the extended fault effect can be clearly detected after removing the gear contribution using DRS and comparing the power spectra at a cyclic frequency that matches the shaft speed. The agreement between the simulated and measured signals shows the robustness of the developed model and its suitability for testing new diagnostic algorithms, as well as prognostic algorithms.

Acknowledgements

This work is supported by the Australian Defence Science and Technology Organization (DSTO). The Authors would like to thank Jerome Antoni for supplying the Matlab® Code for both the (SCF) and the (DRS).

References

Antoni, J., and Randall, R.B. (2006): The Spectral Kurtosis Application to the Surveillance and Diagnostics of Rotating Machines. Mechanical Systems and Signal Processing, 20(2), pp.308-331.

Antoni J. and Randall R.B. (2002): Differential diagnosis of gear and bearing faults, Journal of Vibration and Acoustics, 124, pp.165-171.

Bruce T. Kuhnell. (September 2004): Wear in Rolling Element Bearings and Gears - How Age and Contamination Affect Them. Machinery Lubrication Magazine, Monash University

Du, S. (1997): Dynamic Modelling and simulation of Gear Transmission Error for Gearbox Vibration Analysis. PhD Dissertation, UNSW, Sydney.

Endo, H. (2005): A study of gear faults by simulation, and the development of differential diagnostic techniques. PhD dissertation, UNSW, Sydney.

Feng, N.S, Hahn, E. J and Randall, R. B. (2002): Using transient analysis software to simulate vibration signals due to rolling element bearing defects, Proceedings of the 3rd Australian congress on applied Mechanics, 689-694, Sydney.

Fukata, S, Gad, E.H., Kondou, T., Ayabe, T. and Tamura, H. (1985): *On the Vibration of Ball Bearings*. *Bulletin of JSME*, 28 (239), pp. 899-904.

Gardner, W.A. (1986) :Introduction to Random Processes With Application to Signals and Systems, Macmillan.

Gao, Y. and Randall, R. B. (2000): Simulation of Geometric, Static and dynamic Gear Transmission Errors. Report CEVA-2000-01, Centre of Expertise in Vibration Analysis, UNSW, Sydney.

Harris, F.J. (1966): *Rolling Bearing Analysis I*, John Wiley, New York, pp. 148

Ho, D. (1999): Bearing Diagnostics and Self-Adaptive Noise Cancellation. PhD dissertation, UNSW

Ho, D., and Randall, R.B (2001):Optimization of Bearing diagnostic Techniques Using Simulated and Actual Bearing Fault Signals. Mech .Syst. Signal Process. 14(5) pp. 763-788.

Liew, A., Feng, N. S. and Hahn, E. J. (2002): Transient rolling element bearing systems, Trans. ASME Turbines and Power, 124(4), pp. 984-991.

McFadden, P. D., and Smith, J.D., (1984 A): Vibration Monitoring of Rolling Element Bearings by the High Frequency Resonance Technique A Review. Tribol. Int., 117(1), pp.3–10.

McFadden, P. D., and Smith, J.D., (1984 B): Model for the Vibration Produced by a single Point Defect. Journal of Sound and vibration. 96, No. 1, pp. 69-82

Randall, R. B., Antoni, J., and Chobsaard, S., (2001): The Relationship Between Spectral Correlation and Envelope Analysis in the Diagnostics of Bearing Faults and other Cyclostationary Machine Signals. Mech. Syst. Signal-Process. 15(5) pp. 945–962.

Sawalhi, N., and Randall R.B. (2005): Spectral Kurtosis Optimisation for rolling element bearings, 8th International Symposium on Signal Processing and Applications, Sydney.

Sawalhi, N., Randall R.B and Endo H. (2006 A): Simulating gear and bearing interactions in the presence of faults: paper to be presented at the 7th IFToMM-Conference on Rotor Dynamics, Vienna, Austria, 25-28 September 2006.

Sawalhi, N., Randall R.B and Endo H. (2006 B): Gear and bearing fault simulation applied to diagnostics and prognostics, Proceedings of the 19th International COMADEM, Luleå, Sweden, pp.399-408.

Sweeney, P. J. (1994): *Transmission error Measurement and Analysis*. PhD Dissertation, UNSW.

Wu, J. (2002): *Rotation Invariant Classification of 3D Surface Texture Using Photometric Stereo*, PhD Dissertation, School of Mathematical and Computer Sciences Heriot-Watt University, Edinburgh.